Biophysical Journal

Mechanical regulation of neurite polarization and growth – A computational study

M.A.H. Jakobs,[1] K. Franze,[1] and A. Zemel,[2,*]

ABSTRACT The densely packed microtubule (MT) array found in neuronal cell projections (neurites) serves two fundamental functions simultaneously: It provides a mechanically stable track for molecular-motor based transport, and produces forces which drive neurite growth. The local pattern of MT polarity along the neurite shaft has been found to differ between axons and dendrites. In axons, the neurons' dominating long projections, roughly 90% of the MTs orient with their rapidly growing plus-end away from the cell body while in vertebrate dendrites their orientations are locally mixed. Molecular motors are known to be responsible for cytoskeletal ordering and force generation, but their collective function in the dense MT cytoskeleton of neurites remains elusive. We here hypothesized that both the polarity pattern of MTs along the neurite shaft, and the shaft's global extension are simultaneously driven by molecular motor forces and should thus be regulated by the mechanical load acting on the MT array as a whole. To investigate this, we simulated cylindrical bundles of MTs that are cross-linked and powered by molecular motors by iteratively solving a set of force balance equations. The bundles were subjected to a fixed load arising from actively generated tension in the actomyosin cortex enveloping the MTs. The magnitude of the load and the level of motor-induced connectivity between the MTs have been varied systematically. With increasing load and decreasing motor-induced connectivity between MTs, the bundles became wider in cross section, extended more slowly, and the local MT orientational order was reduced. These results reveal two novel mechanical factors which may underly the distinctive development of the MT cytoskeleton in axons and dendrites – the cross-linking level of MTs by motors, and the load acting on this cytoskeleton during growth.

Statement of significance

A fundamental question of neurobiology is how the distinctive polarity profile of the microtubule array in neuronal cell projections establishes. We present computer simulations of cylindrical microtubule bundles cross-linked and powered by molecular motors; the bundles were subjected to opposing load resulting from actomyosin contractility in the surrounding cytoskeleton. The level of motor-induced connectivity between the microtubules and the load are found to be two determining factors of the bundles' growth and structural characteristics. Highly connected microtubule-motor-bundles efficiently expanded and sorted, forming uniformly polarized bundles, as found in axons. In contrast, loosely connected bundles failed to expand and sort, remaining short and mixed as in dendrites. These calculations provide important insight into the mechanical regulation of neuron development and growth.

1. Introduction

Axons and dendrites (together referred to as neurites) are the mature projections of neurons that transmit and receive information in the form of electrical signals. In contrast to dendrites, which remain short ($\approx 100\mu m$ long) and highly branched, axons may grow $mm - m$ long to reach their target site(s). These extreme axonal dimensions require sophisticated mechanisms that drive axonal growth and molecular transport to ensure proper supply while navigating through the complex extracellular environment. Neurites comprise a densely packed microtubule (MT) cytoskeleton that functions as a substrate for the transport of newly synthesized proteins, organelles, and RNA by molecular motor proteins (1). The MTs are polar filaments, having a rapidly polymerizing plus-end, and a more stable minus-end (1). Molecular motors, such as kinesins and dyneins, recognize this polarity and preferentially move in one direction on the filament. While in axons, most MTs orient uniformly with their plus-ends away from the cell body (enabling efficient transport away from and towards the cell body), in dendrites, this structural organization is not conserved. In vertebrates, the dendritic MT array is locally mixed with MTs pointing in either direction (2, 3), while in *Drosophila melanogaster* and *Caenorhabditis elegans* the MTs point their minus-ends away from the cell body ('minus-end-out') (4, 5).

Apart from serving as tracks for directed molecular transport, the MT cytoskeleton also plays part in generating pushing forces that drive neurite outgrowth (6). In addition to polymerization forces exerted by peripheral MTs at the growth-cone (GC) leading edge, experiments indicate that MTs also contribute to growth via their interaction with molecular motors, which slide the MTs along the membrane (7, 8) or past each other (9, 10), to eventually extend the MT cytoskeleton forward (7, 9–12).

doi: 10.1529/biophysj.106.090944

In particular, experiments have identified dynein (7, 11, 12) and kinesin-1 (7–9) to be essential for neurite outgrowth. Common to both motors is their tendency to dimerise asymmetrically with a cargo domain on one end of the molecule and a moving domain on the other; this structural asymmetry has been shown to be essential for the motors ability to expand parallel bundles of MTs (see (13) and references therein). An important aspect of the molecular motors' directional gliding on the filaments, is that the forces they apply lead to filament sorting. The minus-end directed motor dynein, has been suggested to sort neuronal MTs by sliding plus-end-out MTs away from the cell body and minus-end-out MTs back into the cell body, thereby establishing the observed uniform MT polarity of the axon (7, 10, 14). In contrast, attenuated dynein activity, and/or enhanced kinesin activity have been proposed to explain the mixed MT polarity of vertebrate dendrites (7, 8, 10, 15).

The molecular motor-generated forces that push the MTs into the GC are opposed by an actively generated load arising from the actomyosin cytoskeleton that envelops the MTs (see Fig.1) (11, 12, 16–20). Consistently, inhibition of myosin II motor activity (12, 21) or interference with the neurites' actin cytoskeleton (22–24) have been shown to facilitate neurite outgrowth, while depletion of MTs from the neurite core or inhibition of dynein or kinesin-1 molecular motors resulted in axon retraction and impaired growth (9, 11, 12, 25, 26). Because, however, F-actin and myosin II are also implicated in GC motility, their inhibition also yielded opposite effects on neurite outgrowth (27, 28). The mechanical force balance in the neurite cytoskeleton has also been studied by applying external pulling forces on the cell membrane or GCs of emerging neurites. Threshold forces of $\approx 1000pN$ in PC12 cells (29, 30) and $15 - 100pN$ in chick forebrain neurons (31) have been reported to facilitate stable axon outgrowth, presumably reflecting the load which normally suppresses the extension and growth of neuronal processes.

Previous theoretical models (8, 10, 13, 32, 33) and experiments (10, 12, 34, 35) have demonstrated that molecular motors can sort unorganized MT bundles as well as generate expansive forces against a resisting load. However, the effects of the load on the MT array expansion and sorting during growth, are poorly understood. We here present a computational study of the consequences of the load on expanding bundles of MTs that are cross-linked by molecular motors and identify an important factor that enters the force balance calculation - the level of MT connectivity by motors (governed by χ below). We demonstrate that these two factors (force and MT connectivity) play important roles in dictating the structural and growth characteristics of the MT bundles. We define the local MT polarity along the bundle axis by the local excess of plus-end-out MTs over minus-end-out ones. Bundles subjected to stronger loads are shown to require more filaments in a cross-section to overcome the load and thus become wider and extend more slowly. With a higher level of motor connectivity between the filaments,

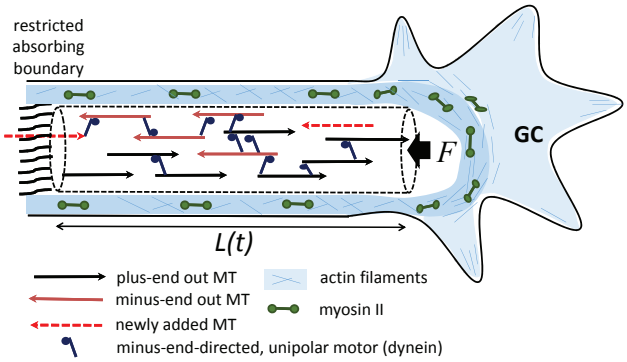

FIGURE 1 Schematic illustration of major elements considered in the model. On the left is the neurite shaft comprising the cross-linked MT bundle that expands as asymmetric (unipolar) motors (dynein) slide the filaments. Filaments reaching the left boundary get absorbed into the cell body with some probability which accounts for the restricted permeability of the entangled meshwork of cytoskeletal filaments (and organelles) present at the widened entry to the cell body (16, 36). The MT bundle is subjected to a restoring (normal) force F on the right boundary arising from the actomyosin cytoskeleton enveloping the MTs (17, 18, 37). New MTs (dashed arrows) of either polarity enter arbitrary points in the bundle with a frequency ω_{in}. Adjacent MTs may or may not be cross-linked by motors. The probability that an overlapping region between adjacent MTs be cross-linked by motors is given by χ.

the bundles narrow in cross-section and grow more quickly while the MTs efficiently sort to form extended, thin and uniformly-polarized bundles, as found in axons. In contrast, loosely connected bundles fail to organize and expand against a load, and result in short, wide and locally mixed bundles, as found in vertebrate dendrites (2, 3). We also demonstrate that the load may play a role in clearing the neurite entry from "ill" oriented minus-end-out MTs that accumulate in that region due to their retrograde transport along the neurite shaft.

2. Materials and Methods

Cylindrical bundles of MTs, cross-linked by minus-end directed unipolar molecular motors (e.g., cytoplasmic dynein) were simulated with one end (the distal GC end) subjected to an opposing normal load, F, and the other end containing an entangled meshwork of cytoskeletal filaments (16, 36) (and organelles) that restrict MT absorption into the cell body while mechanically supporting the load. A similar algorithm has previously been used to investigate the sorting dynamics of force-free bundles (32) and then extended to investigate the expansion dynamics and force generation of parallel bundles using an impermeable left boundary (13). The impact of a load on the growth and establishment of MT polarity profile along neurites'-like MT-motor bundles, that are subjected to a load on their one end and open to MT exchange on

their other end, has not yet been studied. The simulation algorithm including the implementation of the boundary conditions and choice of parameters are described in detail in the supporting information; we here outline the methodology and its major assumptions.

Neuronal MTs vary in length and their length distribution broadly varies between neuron types, animal species and developmental stages (38); a range between $1-30\mu m$ has been reported for cultured rat hippocampal neurons (39), between $3-10\mu m$ in C-elegans motor neurons (40), and much longer MTs, $100 - 400\mu m$, were reported in adult sensory neurons in vivo (41). As these data are limited and the mechanisms controlling the length distribution are still not fully understood (42), we here assumed, for simplicity, that all filaments have the same length, $l = 10\mu m$, and the consequences of varying l are examined in the supporting information (see Fig. S3). The filaments were arranged on a hexagonal lattice in the y-z plane and their position along the x-axis was propagated iteratively by solving a set of force-balance equations for the forces and velocities of all filaments in the bundle, as described in detail in the supplementary information. To investigate how the sliding dynamics and steady-state properties of MTs in the bundle are dictated by the motor-induced connectivity between MTs, we have defined the probability χ that a given overlap region between two adjacent MTs (independently of their orientations) is cross-linked by molecular motors, and have simulated MT motion for varying values of χ. Motors within the same overlapping domain between MTs were assumed to be bound with the same orientation with respect to the MTs (see Fig. 1) since our calculations have indicated that in this configuration the motors more efficiently cooperate to extend the bundle (13) and some evidence for this configuration exists (43, 44). Explicit account of other MT accessory proteins (MAP)s and other types of motor proteins has been neglected for simplicity (however, their implicit effects are discussed below). The initial bundle had a length $L_0 = 15\mu$m and comprised 20 MTs whose centers were randomly distributed along the x-axis and the hexagonal lattice in the y-z-plane. The MT orientation was chosen at random with equal probability. The motion of all MTs was then simulated while new MTs, with randomly chosen orientation, were added at a fixed rate, $\omega_{in} = 0.02\text{sec}^{-1}$, to random positions along the bundle length, to mimic either localized events of MT nucleation and severing within the bundle or transport of MTs from the cell body (1, 10, 15) (see Fig. 1). The fixed rate of mass addition was motivated by the observation that neurite growth rates are constant (30). This resulted in bundles with $1 - 8$ MTs pre cross-section, applicable to the thin neuronal processes of insects (7), worms (45) and other small animals (46); in the supporting information (Fig. S4) we show that our conclusions also hold with thicker bundles obtained with stronger forces and higher inward fluxes of MTs.

3. Results and Discussion

3.1 *Effects of the load and MT-motor connectivity on bundle growth*

The gliding forces exerted by the motors on the MTs simultaneously act to expand the bundle against the load and sort the filaments according to their polarity. Fig. 2 demonstrates the predicted effects of the load, F, and χ, on the bundles' growth speed, and MT polarity profile that established along their length. As seen in panel 2A, beyond a period of few seconds, the mean bundle length $\langle L\rangle$ increased at a fixed speed that decreased with the load on the bundle. The mean growth speed scaled as $d\langle L\rangle/dt \sim 1/F - const$; a similar scaling has been obtained with parallel bundles of filaments (13) but contained no constant term since the left boundary was impermeable (see below). Here $\langle\cdots\rangle$ denotes ensemble averaging over thousands of bundle trajectories. To explain this scaling, we note that the overall MT volume is proportional to

$$L\bar{m} = Nl, \tag{1}$$

where N is the evolving number of MTs, l their lengths, and $\bar{m}$ is the length-averaged number of MTs in a cross-section. During linear growth, $\bar{m}$ adjusted to the load and maintained a fixed value that scaled as $\bar{m} \sim F$, for $F > 10pN$ (Fig. 2B); taking the time derivative from Eq. 1 one finds:

$$\frac{dL}{dt} = \frac{l(\omega_{in} - \omega_{abs})}{\bar{m}} \tag{2}$$

Here, $\omega_{in} = dN_{in}/dt$ is the insertion rate of MTs into the bundle, $\omega_{abs} = dN_{abs}/dt$ is the rate of MT absorption into the cell body, and $dN_{in}/dt - dN_{abs}/dt = dN/dT$ is the total rate of change in the number of MTs. We found ω_{abs} to linearly scale with the load, causing the second term on the right hand side of Eq. 2 to be force-independent. Accordingly, in our simulations bundles subjected to stronger loads became wider and grew more slowly. This is supported by a number of experimental observations: (i) that thinner neurites grew faster than thicker ones (47), (ii) that external pulling of the GC away from the cell body (i.e., in the direction that reduces the load on the MTs) increased neurite growth speed (30), (iii) that myosin II inhibition (12, 21), F-actin depolymerization (22, 23) facilitated growth, and (iv) the evidence that dendrites are somewhat wider than axons (48) (although width control may have multiple mechanisms).

Another factor that significantly affected the bundles' growth speed was the motor-induced connectivity between the MTs, dictated by χ. When χ was reduced, fewer MTs got pushed by motors and more MTs accumulated in a cross section to balance the load (Fig. 2B); consequently the speed of growth decreased (Fig. 2C). We found $\bar{m}$ to scale as $\bar{m}_a/\sqrt{\chi}$, and therefore $d\langle L\rangle/dt = l(\omega_{in} - \omega_{abs})/\bar{m} \sim \sqrt{\chi}$, where $\bar{m}_a \sim F$ is the number of MTs in a cross section that are actively powered by unipolar motor proteins via interaction with other MTs. These findings are qualitatively consistent

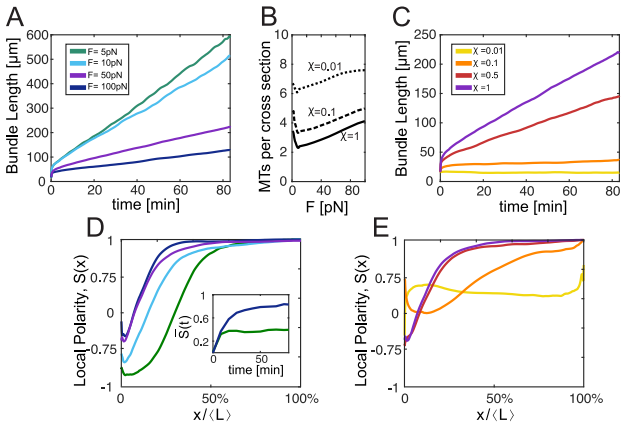

FIGURE 2 The effects of F and χ on bundle growth and polarity. (A) and (C) show the evolution of bundle length for varying levels of F and χ, respectively; green to blue correspond to $F = 5, 10, 50, 100$pN with $\chi = 1$; yellow to purple correspond to $\chi = 0.01, 0.1, 0.5, 1$ with $F = 50$pN. (B) shows the effect of the load on mean number of MTs per cross-section for varying levels of χ. The load on the bundle dictates its width and thereby its growth speed. (D) and (E) show the effects of F and χ on the scaled MT polarity profile $S(x)$ at $t = 80$ min; color coding is as in (A) and (C); the inset in (D) shows that the length-averaged order parameter, $\bar{S}(t)$, stabilizes within ≈ 10 min. The load on the bundle restrains growth and biases the polarity profile at the neurite entry. Highly interconnected MT-bundles (large χ) more quickly expand (taper) and polarize under load, while loosely connected bundles fail to grow and remain short, wide, and mixed.

with the experimental observation that a down-regulation of dynein motors caused axons to retract from weakly adhesive substrates (11) and led to a slowing down of neurite outgrowth (12).

3.2 *Effects of the load and MT-motor connectivity on bundle polarity*

To conveniently examine how F and χ govern the MT polarity profile along the bundle, we defined the normalized factor (order parameter):

$$S(x) = \left\langle \frac{n_R(x) - n_L(x)}{n_R(x) + n_L(x)} \right\rangle, \qquad (3)$$

where, $n_R(x)$ and $n_L(x)$, denote the local number of MTs whose plus-ends point to the right (GC direction) and left (cell body direction), respectively. $S(x) = 1$ and $S(x) = -1$ imply that the bundle is locally polarized, with plus-ends to the right and left, respectively, and $S(x) = 0$ implies a locally mixed region in the bundle. To analyze the changes in the profile of the order parameter during growth, we normalized the x-axis by the overall length of the bundle and examined the order parameter as a function of $x/\langle L \rangle$. The scaled profile was found to settle at a steady-state within few tens of minutes (see Fig. S1) - at which the curves plotted in Fig. 2D-E were calculated ($t = 80$ min). The length averaged order parameter $\bar{S}(t) = 1/L(t) \int S(x,t)\, dx$ stabilized within ≈ 10 min (see inset in panel 2D).

The effect of the load on the polarity profile, $S(x/L)$ is shown in panel 2D for different values of F, in case of high cross-linking probability, $\chi = 1$; the qualitative shape of all curves is similar. Close to the cell-body (left end of the bundle), the bundles are enriched with minus-end-out MTs (thus $S < 0$). Further away, the MT polarity profile is graded, until the bundles eventually organize with all MTs pointing their plus-ends towards the GC ($S = 1$). This graded polarity profile is consistent with the results of Sharp et al. (15) and Stepanova et al., (49) who found higher percentages of plus-end-out MTs distally from the cell body. The monotonic increase of the order parameter with the distance to the cell body arises due to the directed retrograde-transport and gradual accumulation of minus-end-MTs from all points along the shaft length. As the force on the bundle increases, the rate of MT absorption into the cell body (ω_{abs}) also increases. Consequently, the accumulated population of minus-end-out MTs next to the left boundary diminishes with the load on the bundle. This explains why both the length of the domain where $S(x) < 0$, and the absolute value $|S(x)|$ (i.e., of the local MT polarity) in that region, decrease as the load increases. In the limit of very weak forces ($F \lesssim 5pN$, see movie 4 and the corresponding kymograph in Fig. S2C) we obtained a bipolar bundle having minus-end-out MTs segregated next to the left boundary and plus-end-out MTs next to the right boundary, similar to those found in our previous study of force free bundles (32). We obtained more profound enrichment of minus-end-out MTs at the neurite entry also when simulating bundles with shorter MTs (Fig. S3). This resulted because shorter MTs get transported more quickly down the neurite shaft. This suggests an important role for the load in axon formation since it is found to contribute to the sorting out of "ill" oriented (minus-end-out) MTs from the neurite entry.

The effect of χ on the bundles' MT polarity profile is shown in panel 2E. Decreasing χ is seen to lower the absolute value of the order parameter. For sufficiently small χ, we obtained bundles that were mixed throughout (yellow curve); these bundles also failed to grow since the motor induced forces also act to expand the bundle. These results are consistent with the demonstration that minus-end-out MTs accumulate in the axon upon dynein inhibition (10).

To recapitulate the effects of χ and F on the bundles' structural characteristics, we ran our simulations with loads ranging between 1-150pN and χ between $0 - 1$. The results are summarized in Fig. 3 in the form of two "phase" diagrams, showing the MT bundle length L (Fig. 3A) and the length-averaged order parameter $\bar{S} = (1/L) \int S(x) dx$ (Fig. 3B) as a function of F and χ at $t = 80$ min, beyond which both the growth speed and the MT polarity profile did not change (Fig. 2 and Fig. S1). The diagrams reveal four

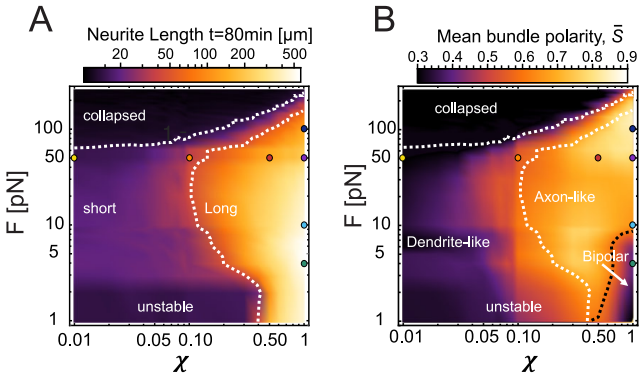

FIGURE 3 : Diagrams recapitulating the effects of χ and F on (A) bundle length $\langle L \rangle$, and (B) mean polarity $\bar{S}$, as calculated at $t = 80$ min, beyond which the growth speed and $\bar{S}$ were stationary. White lines in both panels represent contours of equal bundle length ($20\mu m$ and $100\mu m$). The colored dots correspond to the respective colored curves in Fig. 2. Three regimes are distinguished in (B), see text for details. At low χ, MT bundles are short and mixed as found in vertebrate dendrites. Axon-like, long and uniformly polarized bundles are obtained with sufficient motor-induced connectivity between MTs ($0.1 \lesssim \chi < 1$) and intermediate force ($10 \lesssim F < 100pN$) that is low to enable growth but not too low to prevent accumulation of "ill" oriented (minus-end-out) MTs at the neurite entry. With high connectivity, $\chi \approx 0.5 - 1$, and weak force, $F \lesssim 10pN$, the bundles elongate rapidly and taper while the MTs segregate in two sub-bundles of opposite polarity along the bundle axis; minus-end-out and plus-end-out MTs accumulate next to the neurite entry and GC, respectively.

distinct domains which we highlight in panel 3B:
(i) At low χ ($\lesssim 0.5$) and $1 \lesssim F \lesssim 3$pN, we obtained highly unstable bundles that rapidly tapered down to $1-3$ MTs per cross section, until frequently a critical MT-MT connection got disconnected and the bundle collapsed and regrew again. These bundles remained short on average and typically with mixed polarity (see SI movie 1 and the corresponding kymograph in Fig. S2D).
(ii) For $\chi \lesssim 0.1$ and $3 \lesssim F \lesssim 50$pN we obtained short and mixed bundles that failed to grow and polarize, consistent with those found in vertebrate dendrites (2, 3) (cf. yellow and orange curves in Fig. 2, SI movie 2 and the corresponding kymograph in Fig. S2B).
(iii) With $\chi \gtrsim 0.1$ and $10 \lesssim F \lesssim 100$pN, the motor activity was efficient in sorting the MTs and expanding the bundles against the load. We consequently obtained long and uniformly polarized MT bundles as found in axons (3) (cf. red, violet, and dark blue curves in Fig. 2, SI movie 3, and the corresponding kymograph in Fig. S2A).
(iv) With $\chi \approx 0.5 - 1$ and $F \lesssim 10$pN, we obtained rapidly extending thin bundles that segregated along their axis into two sub-bundles of opposite polarity (cf. green curve in Fig. 2, SI movie 4, and the corresponding kymograph in Fig. S2C). MTs close to the cell body oriented with their plus-ends towards the cell body and those further away oriented in the opposite direction. Unlike in the low χ regimes (i) and (ii) were $\bar{S}$ was low because the bundles were locally mixed ($S(x) \lesssim 0.7$), the bundles here had low $\bar{S}$ since the averaging of $S(x)$ over the bundle length integrated local regions with opposite polarity ($S(x) \approx \pm 0.9 - 1$). This unique bidirectional segregation of MTs occurred because the load was insufficient to effectively push the accumulating minus-end-out MTs into the cell body.

We obtained similar trends and bundle types also with larger MT-motor bundles that comprised tens of MTs per cross-section and hundreds of MTs in total, see Fig. S4 and SI movies 5, 6.

4. Conclusions

Our calculations highlight two mechanical factors which may govern the growth speed, width and MT polarity profile of growing neurites: the magnitude of the load upon the MTs, F, and the motor-induced connectivity between the MTs, as governed by χ. Enhanced load slowed down bundle extension since newly added MT mass distributed radially to balance the load rather than axially to extend the neurite. This explains the common observation that thinner neurites grow faster than thicker ones (47), that myosin inhibition (12, 21), actin depolymerization (22, 23) and external GC pulling (away form the cell body) (30) were shown to accelerate growth, and consistent with the evidence that dendrites have larger diameters than axons (48). On the other hand, the bundles' capacity to withstand a load also depends crucially on the motor-induced connectivity between the MTs; bundles with poor connectivity (small χ) became wide in cross section and failed to grow. Neurites comprise numerous other MAPs that passively cross-link the MTs and provide further structural support. However, they alone are insufficient to extend the neurite nor provide stability on long time scales. In order to expand and/or to withhold a long-standing load, the MTs must be cross-linked by motor proteins which exploit ATP molecules to actively counter the load. Indeed, experiments show that interference with dynein motor activity leads to neurite retraction in otherwise intact neurites, despite the presence of other passive MAPs (11, 12).

Moreover, the gliding forces of the motors also act to sort the MTs according to their polarity since their motion on the filaments is directional. In our simulations, "mixing" of MTs was achieved via constant addition of new MTs with either polarity to arbitrary points along the bundle. Thereby accounting for few possible processes that might take place simultaneously in neurites (10), including transport of MTs by differently directed molecular motors, local MT nucleation, severing of long MTs and flipping of short ones. Both χ and F were found to affect MT sorting along the bundle. In loosely connected bundles (small χ) the MTs remained

with mixed polarity and failed to expand against the load. In contrast, highly connected bundles could expand against the load and polarize uniformly all along their length. Thus, the level of the MT-motor connectivity may be a determining property in the establishment of neurites' major structural characteristics since it is found here to dictate the bundles' length, width and axial MT polarity profile.

We also found the load to have an important effect on the MT polarity profile. To obtain the uniform polarity observed in axons, the load needed to exceed a minimum level that could counter the accumulation of "ill" oriented minus-end-out MTs at the neurite entry and push them into the cell body. This minimum level of force generally increases with the influx of MTs to the bundle (ω_{in}) and the transport speed of the minus-end-out MTs in the neurite shaft. Consequently, bundles comprising shorter MTs accumulated minus-end-out MTs more profoundly next to the neurite entry (see Fig. S3) since their transport down the bundle axis was faster. This suggests that the load on the neurite MT cytoskeleton should be optimized in some regime, which on the one hand enables growth, and on the other hand is sufficiently strong to withdraw accumulating ill-oriented MTs into the cell body to ensure proper MT polarization.

Multiple factors may regulate the binding of dynein molecular motors to the MTs. In particular, the various MAPs that decorate the MT array in neurites are likely candidates. Axons and dendrites have been shown to differ in their MAP content; axons are rich in tau and MAP2C, and dendrites in MAP2 (46). The effects of MAPs on molecular motor activity have been investigated in motility and binding assays as well as in single molecule experiments. While at high MAP/tubulin ratios dynein binding to MTs (50) and gliding speed (51) are reduced, MAP2 and to a lesser degree tau, were shown to sterically inhibit dynein gliding in motility assays in vitro (52). Interestingly, Chen et al. (46) found that the mean spacing between MTs differs between axons and dendrites, being $\approx$ 2-fold smaller ($\approx$ 30nm) in axons than in dendrites; for comparison the MT spacing in dynein-induced MT bundles in vitro is $\approx$ 30nm as well (44). It is thus tempting to speculate that through their steric modulation of the inter-MT separation, MAPs might govern the motor-induced connectivity between MTs, and in this way modulate the arrays' capacity to withstand the load and the molecular motors' ability to sort the MTs.

The loss of cytoskeleton stability and collapse of neuronal processes is one of the hallmarks of neurodegenerative diseases such as Alzheimer's and Parkinson's (53), and both MAPs and dynein dysfunctions have been implicated in the progression of these diseases (42, 54, 55). We have quantitatively shown here that the motor-induced connectivity between the MTs may play a crucial role in establishing neurite mechanical stability and polarity. Whether and precisely how this property is tuned by MAPs, is an intriguing question awaiting further experimental and theoretical investigation.

AUTHOR CONTRIBUTION

A.Z and M.A.H.J wrote the simulation code, M.A.H.J ran the calculations, M.A.H.J, K.F and A.Z designed the work and wrote the paper.

ACKNOWLEDGEMENTS

M.A.H.J acknowledges a Wellcome Trust Research Grant, 109145/Z/15/Z. K.F acknowledges funding from the European Research Council (Consolidator Award 772426 to KF) and A.Z thanks the Eliyahu and Tatiana Leszcynski fund for their support.

SUPPLEMENTARY MATERIAL

An online supplement to this article can be found by visiting BJ Online at http://www.biophysj.org.

REFERENCES and FOOTNOTES

1. Kapitein, L. C., and C. C. Hoogenraad, 2015. Building the Neuronal Microtubule Cytoskeleton. *Neuron* 87:492–506.
2. Baas, P. W., M. M. Black, and G. A. Banker, 1989. Changes in microtubule polarity orientation during the development of hippocampal neurons in culture. *The Journal of cell biology* 109:3085–3094.
3. Yau, K. W., P. Schätzle, E. Tortosa, S. Pagès, A. Holtmaat, L. C. Kapitein, and C. C. Hoogenraad, 2016. Dendrites In Vitro and In Vivo Contain Microtubules of Opposite Polarity and Axon Formation Correlates with Uniform Plus-End-Out Microtubule Orientation. *The Journal of neuroscience : the official journal of the Society for Neuroscience* 36:1071–1085.
4. Yan, J., D. L. Chao, S. Toba, K. Koyasako, T. Yasunaga, S. Hirotsune, and K. Shen, 2013. Kinesin-1 regulates dendrite microtubule polarity in Caenorhabditis elegans. *eLife* 2.
5. Stone, M. C., F. Roegiers, and M. M. Rolls, 2008. Microtubules have opposite orientation in axons and dendrites of Drosophila neurons. *Molecular biology of the cell* 19:4122–4129.
6. Suter, D. M., and K. E. Miller, 2011. The emerging role of forces in axonal elongation. *Progress in neurobiology* 94:91–101.
7. del Castillo, U., M. Winding, W. Lu, V. I. Gelfand, and V. Allan, 2015. Interplay between kinesin-1 and cortical dynein during axonal outgrowth and microtubule organization in Drosophila neurons. *eLife* 4:e10140.
8. Oelz, D. B., U. D. Castillo, V. I. Gelfand, and A. Mogilner, 2018. Microtubule Dynamics, Kinesin-1 Sliding, and Dynein Action Drive Growth of Cell Processes. *Biophysical Journal* 115:1614–1624.

9. Lu, W., P. Fox, M. Lakonishok, M. W. Davidson, and V. I. Gelfand, 2013. Initial neurite outgrowth in Drosophila neurons is driven by kinesin-powered microtubule sliding. *Current biology : CB* 23:1018–1023.
10. Rao, A. N., A. Patil, M. M. Black, E. M. Craig, K. A. Myers, H. T. Yeung, and P. W. Baas, 2017. Cytoplasmic dynein transports axonal microtubules in a polarity-sorting manner. *Cell reports* 19:2210–2219.
11. Ahmad, F. J., J. Hughey, T. Wittmann, A. Hyman, M. Greaser, and P. W. Baas, 2000. Motor proteins regulate force interactions between microtubules and microfilaments in the axon. *Nature cell biology* 2:276–280.
12. Roossien, D. H., P. Lamoureux, and K. E. Miller, 2014. Cytoplasmic dynein pushes the cytoskeletal meshwork forward during axonal elongation. *J Cell Sci* 127:3593–3602.
13. Jakobs, M., K. Franze, and A. Zemel, 2015. Force Generation by Molecular-Motor-Powered Microtubule Bundles; Implications for Neuronal Polarization and Growth. *Frontiers in cellular neuroscience* 9:441.
14. Tanenbaum, M. E., R. D. Vale, and R. J. McKenney, 2013. Cytoplasmic dynein crosslinks and slides anti-parallel microtubules using its two motor domains. *eLife* 2:e00943.
15. Sharp, D. J., W. Yu, and P. W. Baas, 1995. Transport of dendritic microtubules establishes their nonuniform polarity orientation. *The Journal of Cell Biology* 130:93–103.
16. Xu, K., G. Zhong, and X. Zhuang, 2013. Actin, spectrin, and associated proteins form a periodic cytoskeletal structure in axons. *Science* 339:452–456.
17. Tofangchi, A., A. Fan, and M. T. A. Saif, 2016. Mechanism of axonal contractility in embryonic drosophila motor neurons in vivo. *Biophysical journal* 111:1519–1527.
18. Mutalik, S. P., J. Joseph, P. A. Pullarkat, and A. Ghose, 2018. Cytoskeletal mechanisms of axonal contractility. *Biophysical journal* 115:713–724.
19. Recho, P., A. Jerusalem, and A. Goriely, 2016. Growth, collapse, and stalling in a mechanical model for neurite motility. *Phys. Rev. E* 93:032410.
20. de Rooij, R., E. Kuhl, and K. E. Miller, 2018. Modeling the axon as an active partner with the growth cone in axonal elongation. *Biophysical journal* 115:1783–1795.
21. Hur, E.-M., I. H. Yang, D.-H. Kim, J. Byun, W.-L. Xu, P. R. Nicovich, R. Cheong, A. Levchenko, N. Thakor, F.-Q. Zhou, et al., 2011. Engineering neuronal growth cones to promote axon regeneration over inhibitory molecules. *Proceedings of the National Academy of Sciences* 108:5057–5062.
22. Bradke, F., and C. Dotti, 1999. The Role of Local Actin Instability in Axon formation. *Science* 283:1931–1934.
23. Ruthel, G., and P. J. Hollenbeck, 2000. Growth cones are not required for initial establishment of polarity or differential axon branch growth in cultured hippocampal neurons. *Journal of Neuroscience* 20:2266–2274.
24. Marsh, L., and P. C. Letourneau, 1984. Growth of neurites without filopodial or lamellipodial activity in the presence of cytochalasin B. *The Journal of cell biology* 99:2041–2047.
25. Dehmelt, L., P. Nalbant, W. Steffen, and S. Halpain, 2006. A microtubule-based, dynein-dependent force induces local cell protrusions: Implications for neurite initiation. *Brain Cell Biol.* 35:39–56.
26. Lu, W., M. Lakonishok, and V. I. Gelfand, 2015. Kinesin-1–powered microtubule sliding initiates axonal regeneration in Drosophila cultured neurons. *Molecular biology of the cell* 26:1296–1307.
27. Letourneau, P. C., T. A. Shattuck, and A. H. Ressler, 1987. Pull and push in neurite elongation: observations on the effects of different concentrations of cytochalasin B and taxol. *Cell motility and the cytoskeleton* 8:193–209.
28. Miller, K. E., and D. M. Suter, 2018. An integrated cytoskeletal model of neurite outgrowth. *Frontiers in cellular neuroscience* 12:447.
29. Zheng, J., P. Lamoureux, V. Santiago, T. Dennerll, R. E. Buxbaum, and S. R. Heidemann, 1991. Tensile regulation of axonal elongation and initiation. *The Journal of neuroscience* 11:1117–1125.
30. Chada, S., P. Lamoureux, R. E. Buxbaum, and S. R. Heidemann, 1997. Cytomechanics of neurite outgrowth from chick brain neurons. *Journal of Cell Science* 110:1179–1186.
31. Fass, J. N., and D. J. Odde, 2003. Tensile force-dependent neurite elicitation via anti-β1 integrin antibody-coated magnetic beads. *Biophysical journal* 85:623–636.
32. Zemel, A., and A. Mogilner, 2009. Motor-induced sliding of microtubule and actin bundles. *Physical chemistry chemical physics : PCCP* 11:4821–4833.
33. Ravichandran, A., G. A. Vliegenthart, G. Saggiorato, T. Auth, and G. Gompper, 2017. Enhanced dynamics of confined cytoskeletal filaments driven by asymmetric motors. *Biophysical journal* 113:1121–1132.
34. Kapitein, L. C., E. J. Peterman, B. H. Kwok, J. H. Kim, T. M. Kapoor, and C. F. Schmidt, 2005. The bipolar mitotic kinesin Eg5 moves on both microtubules that it crosslinks. *Nature* 435:114.
35. Braun, M., D. R. Drummond, R. A. Cross, and A. D. McAinsh, 2009. The kinesin-14 Klp2 organizes microtubules into parallel bundles by an ATP-dependent sorting mechanism. *Nature cell biology* 11:724.
36. Tas, R. P., A. Chazeau, B. M. Cloin, M. L. Lambers, C. C. Hoogenraad, and L. C. Kapitein, 2017. Differentiation between oppositely oriented microtubules controls polarized neuronal transport. *Neuron* 96:1264–1271.

37. Coles, C. H., and F. Bradke, 2015. Coordinating Neuronal Actin–Microtubule Dynamics. *Current Biology* 25:R677–R691.
38. Leterrier, C., P. Dubey, and S. Roy, 2017. The nano-architecture of the axonal cytoskeleton. *Nature Reviews Neuroscience* 18:713.
39. Yu, W., and P. W. Baas, 1994. Changes in microtubule number and length during axon differentiation. *Journal of Neuroscience* 14:2818–2829.
40. Yogev, S., R. Cooper, R. Fetter, M. Horowitz, and K. Shen, 2016. Microtubule organization determines axonal transport dynamics. *Neuron* 92:449–460.
41. Burton, P. R., 1987. Microtubules of frog olfactory axons: their length and number/axon. *Brain research* 409:71–78.
42. Baas, P. W., A. N. Rao, A. J. Matamoros, and L. Leo, 2016. Stability properties of neuronal microtubules. *Cytoskeleton* 73:442–460.
43. Haimo, L. T., and R. D. Fenton, 1984. Microtubule crossbridging by chlamydomonas dynein. *Cell Motil.* 4:371–385.
44. Amos, L. A., 1989. Brain dynein crossbridges microtubules into bundles. *Journal of Cell Science* 93:19–28.
45. Yogev, S., R. Cooper, R. Fetter, M. Horowitz, and K. Shen, 2016. Microtubule Organization Determines Axonal Transport Dynamics. *Neuron* 92:449–460.
46. Chen, J., Y. Kanai, N. J. Cowan, and N. Hirokawa, 1992. Projection domains of MAP2 and tau determine spacings between microtubules in dendrites and axons. *Nature* 360:674–677.
47. Tomba, C., C. Braïni, B. Wu, N. Gov, and C. Villard, 2014. Tuning the adhesive geometry of neurons: length and polarity control. *Soft Matter* 10:2381.
48. Costa, A. R., R. Pinto-Costa, S. C. Sousa, and M. M. Sousa, 2018. The regulation of axon diameter: From axonal circumferential contractility to activity-dependent axon swelling. *Frontiers in molecular neuroscience* 11:319.
49. Stepanova, T., J. Slemmer, C. C. Hoogenraad, G. Lansbergen, B. Dortland, C. I. De Zeeuw, F. Grosveld, G. van Cappellen, A. Akhmanova, and N. Galjart, 2003. Visualization of microtubule growth in cultured neurons via the use of EB3-GFP (end-binding protein 3-green fluorescent protein). *Journal of Neuroscience* 23:2655–2664.
50. Hagiwara, H., H. Yorifuji, R. Sato-Yoshitake, and N. Hirokawa, 1994. Competition between motor molecules (kinesin and cytoplasmic dynein) and fibrous microtubule-associated proteins in binding to microtubules. *Journal of Biological Chemistry* 269:3581–3589.
51. Vershinin, M., J. Xu, D. S. Razafsky, S. J. King, and S. P. Gross, 2008. Tuning Microtubule-Based Transport Through Filamentous MAPs: The Problem of Dynein. *Traffic* 9:882–892.
52. Lopez, L. A., and M. P. Sheetz, 1993. Steric inhibition of cytoplasmic dynein and kinesin motility by MAP2. *Cytoskeleton* 24:1–16.
53. Luo, L., and D. D. O'Leary, 2005. Axon retraction and degeneration in development and disease. *Annu. Rev. Neurosci.* 28:127–156.
54. Gendron, T. F., and L. Petrucelli, 2009. The role of tau in neurodegeneration. *Molecular neurodegeneration* 4:13.
55. Eschbach, J., and L. Dupuis, 2011. Cytoplasmic dynein in neurodegeneration. *Pharmacology & therapeutics* 130:348–363.